Journal of Materials Chemistry A

RSC Publishing

PAPER

View Article Online
View Journal | View Issue



Cite this: J. Mater. Chem. A, 2013, 1, 2501

# High performance $LiV_{0.96}Mn_{0.04}PO_4F/C$ cathodes for lithium-ion batteries

Xiaofei Sun,[a] Youlong Xu,*[a] Mingrui Jia,[a] Peng Ding,[a] Yanghao Liu[b] and Kai Chen[c]

Received 16th September 2012
Accepted 4th December 2012

DOI: 10.1039/c2ta01338j

www.rsc.org/MaterialsA

The $LiV_{0.96}Mn_{0.04}PO_4F/C$ composite was prepared by partial substitution of vanadium with manganese and *in situ* carbon coating of $LiVPO_4F$ *via* a modified carbothermal reduction route. Rietveld refinement of X-ray diffraction (XRD) patterns shows that the crystalline lattice is smaller than the value reported in the literature. While electron energy loss spectroscopy (EELS) on a selected area of high resolution transmission electron microscopy (HRTEM) demonstrates that Mn is successfully doped into $LiVPO_4F$, X-ray photoelectron spectroscopy (XPS) indicates the co-existence of $Mn^{3+}$ and $Mn^{4+}$. With ~6.29 wt% residual carbon (estimated by thermogravimetric analysis, TGA) included, the specific discharge capacity of $LiV_{0.96}Mn_{0.04}PO_4F/C$ at 0.1 C and 6 C could reach 138 mA h $g^{-1}$ and 98 mA h $g^{-1}$, respectively. The capacity retention after 1000 cycles at 1 C is about 90%, corresponding to only 0.01% loss per cycle. Electrochemical impedance spectroscopy (EIS) shows that the charge transfer resistance ($R_{ct}$) is significantly reduced by Mn substitution, and the lithium diffusion coefficient was calculated to be $1.34 \times 10^{-13}$ $cm^2$ $s^{-1}$, which is an order of magnitude higher than that of pristine $LiVPO_4F/C$. Moreover, $LiV_{0.96}Mn_{0.04}PO_4F/C$ retains 74% of its initial capacity after 500 cycles at 1 C at 65 °C, indicating its potential application at high temperatures.

## 1 Introduction

Environmentally friendly high energy and high power lithium ion batteries (LIBs) are increasingly important for next generation energy storage applications, such as in electronic devices, electric vehicles (EVs) including hybrid electric vehicles (HEVs) and plug-in hybrid electric vehicles (PHEVs), and stationary electricity storage.[1–3] At the same time, safety, cost and lifetime are also key issues for industrial applications of LIBs.[4,5] Polyanion compounds[6–9] containing MO (M = transition metals such as Fe, Mn, Co, Ni, V, *etc.*) octahedra and XO (X = Si, S, P, As, *etc.*) tetrahedra in an open framework structure have shown great potential as cathode materials for LIBs, since the successful demonstration of $LiFePO_4$ in 1997 by Padhi *et al.*[10] In 2003, J. Barker[11] introduced fluorine (F) into the phosphate system as $LiVPO_4F$, which showed promising electrochemical performance, and particularly a higher discharge potential at 4.2 V (*vs.* $Li/Li^+$ hereafter). In addition, J. R. Dahn's group[12] testified the superior thermal stability of charged $LiVPO_4F$ over charged $LiFePO_4$ because of the strong ionic bonding between V and F, as well as the inductive effect of the $PO_4^{3-}$ groups.

$LiVPO_4F$ is isostructural with tavorite ($LiFePO_4OH$) and amblygonite ($LiAlPO_4F$) in the triclinic space group $P\bar{1}$. It is constructed from $PO_4$ tetrahedra and $VO_4F_2$ octahedra, where $PO_4$ shares an O with $VO_4F_2$ and $VO_4F_2$ are connected to each other by F. However, there is still an argument concerning lithium occupancy. Combining Rietveld refinement of X-ray diffraction with solid-state $^{6,7}Li$ NMR analysis, Ellis *et al.*[13] found two distinguishable Li sites in $LiVPO_4F$. On the contrary, only one crystallographic site was determined *via* X-ray diffraction and neutron diffraction by J.-M. Ateba Mba *et al.*[14] Interestingly, lithium re-arrangement during charge/discharge in the first cycle was also observed.[15] Nevertheless, the high discharge potential from the high electronegativity of $PO_4F^{4-}$ together with the moderate specific capacity (156 mA h $g^{-1}$) endows $LiVPO_4F$ with an improved specific energy (655 W h $Kg^{-1}$) compared with $LiFePO_4$ (595 W h $Kg^{-1}$). The main obstacles hindering its commercialization include the difficult preparation of phase-pure $LiVPO_4F$, the low initial discharge/charge efficiency, inferior rate capability and the poor cycling performance. Surface coating and bulk doping are applied to overcome these shortcomings like in other well-known cathode systems such as $LiFePO_4$[8,16,17] and $LiMn_2O_4$.[18–21] Extra carbon[22] is usually generated during the carbothermal reduction (CTR) synthesis[23,24] of $LiVPO_4F$, and aluminum (Al)[25,26] was used to partially substitute V, considering the isostructure of $LiAlPO_4F$ and $LiVPO_4F$. With 10 at% doping, $LiV_{0.9}Al_{0.1}PO_4F$ retained 95% of its initial capacity (105 mA h $g^{-1}$) after 50 cycles at a rate of 1 C. The cyclability was enhanced but the capacity decreased

[a]Electronic Materials Research Laboratory, Key Laboratory of the Ministry of Education, Xi'an Jiaotong University, Xi'an 710049, China. E-mail: ylxuxjtu@mail.xjtu.edu.cn; Fax: +86-29-82665161; Tel: +86-29-82665161

[b]Department of Chemistry, Xi'an Jiaotong University, Xi'an 710061, China

[c]Center for Advancing Materials Performance from the Nanoscale (CAMP-Nano), State Key Laboratory for Mechanical Behavior of Materials, Xi'an Jiaotong University, Xi'an 710049, China

due to the non-activity of $Al^{3+}$ during charge/discharge. It is also noteworthy that Reddy *et al.*[27] have recently demonstrated the stable cycling of bare $LiVPO_4F$ up to 800 cycles as a viable cathode for LIBs.

In this work, 4 at% manganese (Mn) was chosen to substitute vanadium (V) *via* a facile two-step process. Mn is a common transition metal with vast abundance on earth. Moreover, it is electrochemically active among different oxidation states. The influence of Mn doping on the crystalline structure, particle morphology and electrochemical performance of $LiVPO_4F$ was investigated.

## 2 Experimental

### 2.1 Materials preparation

$LiVPO_4F$ was prepared by a traditional two-step carbothermal reduction route. Firstly, $V_2O_5$ was ball milled with $NH_4H_2PO_4$ in stoichiometric amounts, and acetylene black was added with a 20 wt% excess. The mixture was calcined at 750 °C for 5 h in an argon (Ar) atmosphere to prepare $VPO_4$. In the second step, the intermediate $VPO_4$ was mixed with LiF, which was sintered at 700 °C under Ar protection for 2 h to give $LiVPO_4F$. The reactions are given[28] as:

$$V_2O_5 + 2NH_4H_2PO_4 + 2C \rightarrow 2VPO_4 + 2NH_3 + 3H_2O + 2CO \quad (1)$$

$$LiF + VPO_4 \rightarrow LiVPO_4F \quad (2)$$

The unexhausted acetylene black was left either as amorphous carbon or as carbon coating on the surface of $LiVPO_4F$ in the final product, as will be discussed later. The sample is therefore reasonably designated as $LiVPO_4F/C$.

$LiV_{0.96}Mn_{0.04}PO_4F$ was synthesized by a similar approach. Different from previous doping methods,[25,29] the intermediate $V_{0.96}PO4$ was prepared instead of $VPO_4$ in the first step, and stoichiometric $MnO_2$ was added along with LiF in the second step. Likewise, it is represented as $LiV_{0.96}Mn_{0.04}PO_4F/C$.

### 2.2 Characterization

The crystal structure was identified by powder X-ray diffraction (XRD) performed on an X'pert Pro (PANalytical) with Cu Kα radiation ($\lambda = 1.5406$ Å). The lattice parameters were calculated by Rietveld refinement using the High Score Plus software package. X-ray photoelectron spectroscopy (XPS) was collected on a K-Alpha system with a monochromatic Al Kα (1486.6 eV) anode. The deconvolution of narrow scan peaks was conducted by the XPS Peak fit program with a Shirley background and a Gauss–Lorentz (ratio 80 : 20) non-linear curve function. The particle morphology was observed by field emission scanning electron microscopy (FESEM, Hitachi S4800) and high resolution transmission electron microscopy (HRTEM, JEOL 2100F). The electron energy loss spectroscopy (EELS) was carried out along with HRTEM between 480 eV and 680 eV to include the vanadium L edge, the oxygen K edge and the manganese L edge. Thermogravimetric differential thermal analysis (TG-DTA, Netzsch STA 449C) was carried out at a heating rate of 5 °C $min^{-1}$ from room temperature to 800 °C in air to determine the amount of residual carbon. $LiVPO_4F/C$ was taken as the background sample before the thermal test of $LiV_{0.96}Mn_{0.04}PO_4F/C$.

### 2.3 Electrochemical performance

A homogeneous slurry of the active material ($LiVPO_4F/C$ or $LiV_{0.96}Mn_{0.04}PO_4F/C$, 80 wt%), conducting carbon (acetylene black, 12 wt%) and binder (PVDF, 8 wt%) in NMP was cast onto a pretreated aluminum foil by the doctor blade technique. The obtained cathode was dried under vacuum at 80 °C for 12 h. CR2016 coin cells were fabricated in an Ar-filled glove box. Lithium metal was used as the anode, and the electrolyte was 1 mol $L^{-1}$ $LiPF_6$ in EC–DMC (1 : 1) solvent. The galvanostatic charge/discharge was performed on a CT2001A Land Battery Testing System, while the cyclic voltammetry (CV) and the electrochemical impedance spectroscopy (EIS) tests were carried out on a Versatile Multichannel Galvanostat 2/Z (VMP2, Princeton Applied Research). The EIS was collected in the frequency range of $10^{-2}$ Hz to $10^5$ Hz and was fitted by the Zsimpwin program. The high temperature cycling was executed in a RHP-80CT programmable temperature chamber.

## 3 Results and discussion

Fig. 1 shows the XRD pattern of $LiV_{0.96}Mn_{0.04}PO_4F/C$. As has already been pointed out,[12] $Li_3V_2(PO4)_3$ is a common by-product during the synthesis of $LiVPO_4F$, but a little $V_3O_5$ was also found in our sample. Since the content of the impurities is very small, the XRD pattern was refined based on the $LiVPO_4F$ model with one Li site assigned.[14] The agreement of the Rietveld refinement is: $R_p = 3.57$, $R_{wp} = 4.68$, $R_{Bragg} = 1.66$ and $\chi^2 = 7.40$. The calculated lattice parameters are: $a = 5.1670(3)$ Å, $b = 5.3049(4)$ Å, $c = 7.2596(7)$ Å, $\alpha = 107.6014(0)°$, $\beta = 107.9796(0)°$, $\gamma = 98.3932(5)°$, $V = 174.0162(0)$ Å$^3$, $V/Z = 87.0081$ Å$^3$. The unit cell is smaller than the reported value[13,14] due to the smaller ionic radius of Mn ($Mn^{3+}$: 0.066 nm; $Mn^{4+}$: 0.060 nm) than $V^{3+}$

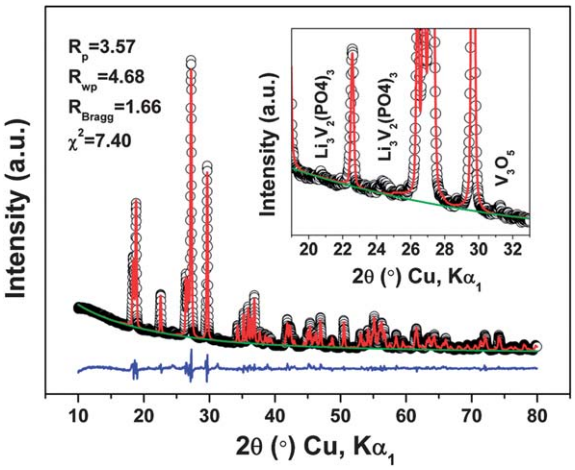


**Fig. 1** XRD pattern of $LiV_{0.96}Mn_{0.04}PO_4F/C$ with Rietveld refinement based on the $LiVPO_4F$ model. The black circles, green line, red line and blue line represent the observed data, background, calculated pattern and the difference pattern, respectively.

 

(0.074 nm). Note that no crystallographic signal associated with carbon was observed which indicates that the residual carbon is mainly amorphous, as will be seen by HRTEM. Fig. 2 shows the Mn and V XPS core level spectra of $LiV_{0.96}Mn_{0.04}PO_4$/C. C 1s was corrected to 284.6 eV to analyze the Mn 2p peaks,[30,31] while O 1s was corrected to 530.0 eV for better analysis of the V 2p peaks.[32,33] The peak intensities of Mn 2p are lower and their noise/signal ratios are also higher due to the small amount of Mn in the material. Deconvolution was precisely carried out by Mn $2p_{3/2}$, Mn $2p_{1/2}$, V $2p_{3/2}$ and V $2p_{1/2}$, with the FWHM (full width at half maximum) less than 4 eV. The results are shown in Table 1. The best fit of the Mn $2p_{3/2}$ and Mn $2p_{1/2}$ spectra gives two BE (binding energy) values. The major peak with a BE of 641.4 eV corresponds to $Mn^{3+}$, and the less prominent one at 643.4 eV corresponds to $Mn^{4+}$. As no detectable $Mn^{4+}$ impurity could be identified by XRD, manganese is thought to be doped in $LiVPO_4F$ at multiple valences ($Mn^{3+}$ and $Mn^{4+}$), which will hopefully increase the phase transformation kinetics of the cathode during charge/discharge by introducing atomic defects.[34] The BE values of V $2p_{3/2}$ and V $2p_{1/2}$ also compare reasonably well with those reported by Reddy *et al.*[27] considering the difference in O 1s reference. It can therefore be seen that most of the vanadium is $V^{3+}$ but a trace amount of $V^{4+}$ is also seen, which possibly comes from $V_3O_5$ according to XRD.

Fig. 3 shows the SEM picture of $LiV_{0.96}Mn_{0.04}PO_4F$/C. The particle size is about 0.8–1.5 μm and is mainly distributed around 1 μm. Moreover, small carbon particles are observed surrounding the $LiV_{0.96}Mn_{0.04}PO_4F$. The high resolution TEM image in Fig. 4(a) indicates that the particle size of the amorphous carbon is about 50–70 nm. Close amplification in Fig. 4(b) verifies the *in situ* carbon coating on the particle surface of $LiV_{0.96}Mn_{0.04}PO_4F$ from the extra carbon during the carbothermal synthesis. The inset of Fig. 4(b) shows the electron energy loss spectroscopy of $LiV_{0.96}Mn_{0.04}PO_4F$ on the selected area of the HRTEM image. The characteristic peak of Mn is validated as well as that of V and O in the energy range of 480–680 eV, demonstrating the successful doping of Mn into $LiVPO_4F$. The carbon content was determined by TGA-DTA, as shown in Fig. 5. The weight loss of ~6.29 wt% from 400 °C to 500 °C with an exothermic peak corresponds well with carbon combustion. The doped Mn and the residual carbon, especially that coated on the surface of the host, are anticipated to improve the conductivity of $LiVPO_4F$, and thus its battery performance.

**Table 1** Overview of peak fit of the XPS of $LiV_{0.96}Mn_{0.04}PO_4F$/C

| Core line | Peaks | BE (eV) | FWHM (eV) | Area (counts eV $s^{-1}$) |
|---|---|---|---|---|
| C 1s | C 1s | 284.5 | 2.03 | 30 070 |
| | C 1s-2 | 285.8 | 3.46 | 3635 |
| Mn $2p_{3/2}$ | $Mn^{3+}$ $2p_{3/2}$ | 641.4 | 2.46 | 1757 |
| | $Mn^{4+}$ $2p_{3/2}$ | 643.4 | 2.58 | 476 |
| Mn $2p_{1/2}$ | $Mn^{3+}$ $2p_{1/2}$ | 653.2 | 2.12 | 600 |
| | $Mn^{4+}$ $2p_{1/2}$ | 654.5 | 2.34 | 231 |
| O 1s | O 1s | 530.0 | 2.51 | 31 404 |
| | O 1s-2 | 530.9 | 2.80 | 453 |
| V $2p_{3/2}$ | $V^{3+}$ $2p_{3/2}$ | 515.4 | 2.72 | 6800 |
| | $V^{4+}$ $2p_{3/2}$ | 516.1 | 2.15 | 217 |
| V $2p_{1/2}$ | $V^{3+}$ $2p_{1/2}$ | 522.7 | 2.96 | 3168 |
| | $V^{4+}$ $2p_{1/2}$ | 523.3 | 3.52 | 93 |

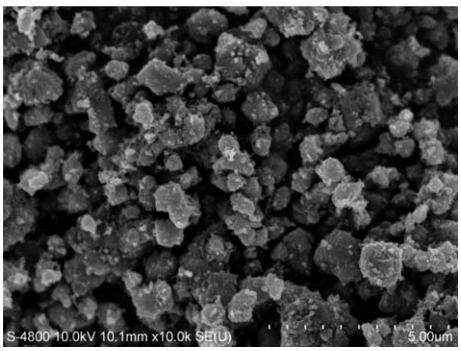


**Fig. 3** FESEM image of $LiV_{0.96}Mn_{0.04}PO_4F$/C.

CR2016 coin cells with Li metal as the anode were made to investigate the electrochemical performance of the $LiV_{0.96}Mn_{0.04}PO_4F$/C composite. The charge/discharge curves at 0.1 C rate (1 C means charge/discharged in 1 h) in the potential range of 2.5–4.6 V are shown in Fig. 6. Combined with the CV curves shown in the inset, the flat profiles with plateaus at 4.32 V and 4.16 V during charge/discharge corroborate the two-phase reaction mechanism.[13] The charge/discharge tails in the

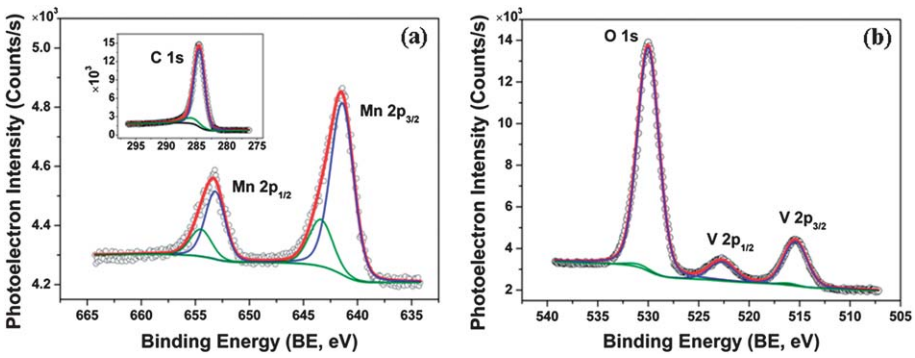


**Fig. 2** XPS spectra of $LiV_{0.96}Mn_{0.04}PO_4F$/C. (a) Mn 2p with C 1s as the reference, and (b) V 2p with O 1s as the reference. The deconvolution of each peak is also shown. The black lines represent the Shirley type backgrounds and the thick red lines over the raw data (circles) are the summations of the deconvoluted contributions.

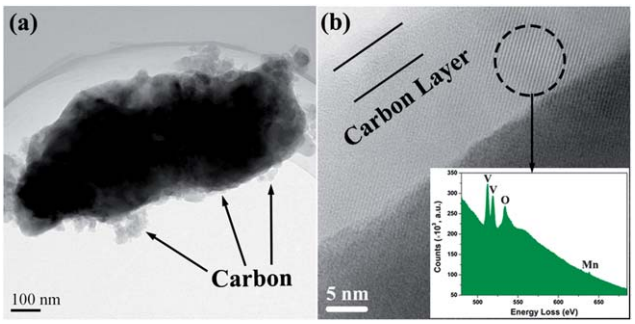


**Fig. 4** HRTEM image of $LiV_{0.96}Mn_{0.04}PO_4F/C$. (a) is magnified in (b), where the inset shows the electron energy loss spectroscopy (EELS) of the selected area.

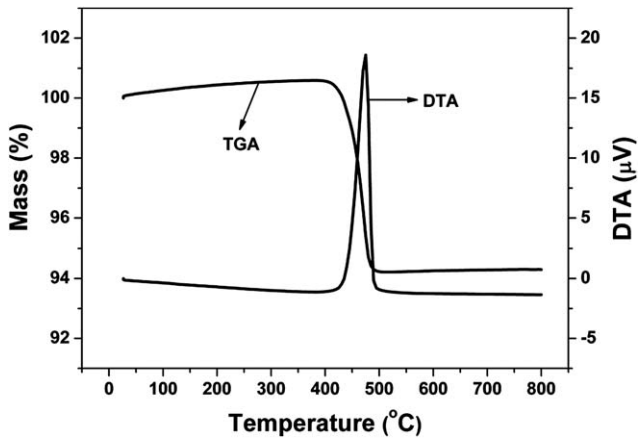


**Fig. 5** TG-DTA curves of $LiV_{0.96}Mn_{0.04}PO_4F/C$ from room temperature to 800 °C at a heating rate of 5 °C $min^{-1}$.

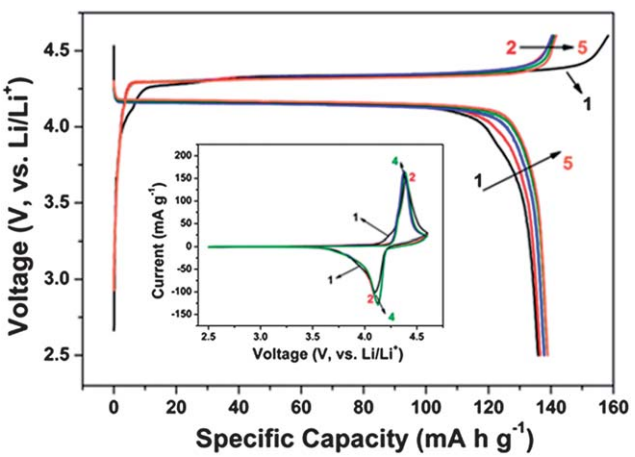


**Fig. 6** Room temperature charge/discharge curves of $LiV_{0.96}Mn_{0.04}PO_4F/C$ at 0.1 C. The inset shows the CV curves at a scanning rate of 0.05 mV $s^{-1}$, while the number indicates the test cycles. The load density of the electrode is 1.92 mg $cm^{-2}$, with the formulation of active material : acetylene black : PVDF = 80 : 12 : 8 (weight).

first cycle may come from the formation of a solid electrolyte interface (SEI)[22,35] especially with residual carbon and impurities in the sample, which also probably causes the slight increase of specific discharge capacity from 136 mA h $g^{-1}$ to 139 mA h $g^{-1}$ with the initial cycling up to the fourth cycle. The details are still not fully understood. Fig. 7 shows the rate performance of $LiV_{0.96}Mn_{0.04}PO_4F/C$ between 3.0 and 4.5 V. The prototype battery was tested at 0.1 C, 0.05 C, 0.2 C, 0.1 C, 0.5 C, 1 C, 6 C, 3 C, 0.1 C, 12 C and back to 0.1 C again successively, with 5 cycles at each rate. As shown in Fig. 7(a), the representative specific discharge capacities are 138 mA h $g^{-1}$, 141 mA h $g^{-1}$, 135 mA h $g^{-1}$, 138 mA h $g^{-1}$, 129 mA h $g^{-1}$, 120 mA h $g^{-1}$, 98 mA h $g^{-1}$, 107 mA h $g^{-1}$, 137 mA h $g^{-1}$, 65 mA h $g^{-1}$ and 132 mA h $g^{-1}$, respectively. To our knowledge, this is the first report of a specific discharge capacity of nearly 100 mA h $g^{-1}$ at 6 C for $LiVPO_4F$ so far. Note that all the specific capacities in this paper are calculated based on the total mass of fluorophosphates and residual carbon, which means that the capacity values could actually be higher if the residual carbon was subtracted from the mass of the active materials. We also believe that these values, especially that at 12 C, could still be increased by optimization of the electrode composition (*e.g.* the ratio of active materials, conductive additives and binders).[8] Meanwhile, the specific discharge capacity exhibits good recovery to 0.1 C after switching to different charge/discharge rates. The same battery was then tested for long term cycling at different rates, as shown in Fig. 7(b). The specific discharge capacity slowly decays from 122 mA h $g^{-1}$ to 116 mA h $g^{-1}$ after 300 cycles at 1 C with a capacity retention of 95%, which is 97% and 96% for the 100 successive cycles at 3 C and 6 C, respectively. The final 20 cycles at 0.2 C show a specific discharge capacity of 130 mA h $g^{-1}$, demonstrating again the good capacity flexibility of $LiV_{0.96}Mn_{0.04}PO_4F/C$. The ultra long term cycling of $LiVPO_4F/C$ with and without Mn doping between 3.0 V and 4.5 V is compared in Fig. 8. The specific discharge capacity of $LiV_{0.96}Mn_{0.04}PO_4F/C$ is 126 mA h $g^{-1}$ and 114 mA h $g^{-1}$ before and after 1000 cycles at 1 C, respectively, corresponding to a capacity retention of 90%, which means a capacity loss of only 0.01% per cycle. Both the capacity and the retention are significantly larger than the highest values reported in the literature.[27] Moreover, the capacity at 0.1 C recovers to its initial value well after the long term cycling. On the other hand, pristine $LiVPO_4F/C$ synthesized under similar conditions without Mn (Fig. 8(b)) loses more than 46% of its initial capacity (91 mA h $g^{-1}$) after 1000 cycles at 1 C.

Electrochemical impedance spectroscopy is a useful technique to study the kinetics of battery materials.[27,36,37] In this work, the cells were charge/discharged for 10 cycles at 0.5 C before EIS tests. The spectra of $LiV_{0.96}Mn_{0.04}PO_4F/C$ and $LiVPO_4F/C$ were collected at the discharged state after an equilibration period of 2 h. The results are shown in Fig. 9. The impedance spectrum of $LiV_{0.96}Mn_{0.04}PO_4F/C$ could be fitted by the equivalent circuit of $R_s(C_{sei}R_{sei})(QR_{ct})(C_eR_e)Z_W$, where $R_s$ represents the resistance of $Li^+$ and electrons passing through the electrolyte, separator, and externals, $C_{sei}$ and $R_{sei}$ are the capacitance and resistance of the SEI layer formed on the surface of the electrode, $Q$(CPE) and $R_{ct}$ are the capacitance and resistance related to charge transfer, $C_e$ and $R_e$ are the capacitance and resistance related to the electron transportation in the active material, and $Z_w$ is the Warburg impedance associated with lithium ion diffusion in $LiV_{0.96}Mn_{0.04}PO_4F/C$, which is

 

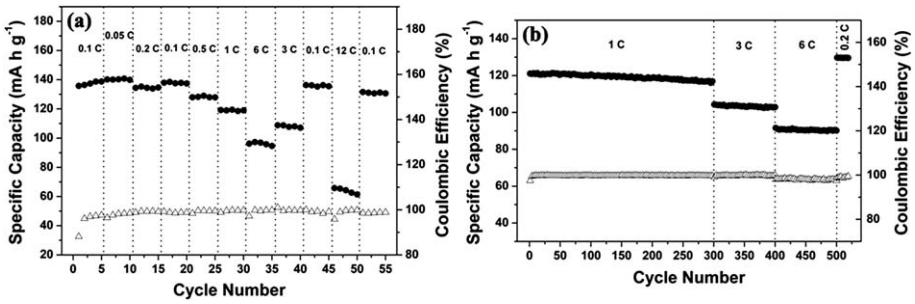


**Fig. 7** Room temperature rate performance of $LiV_{0.96}Mn_{0.04}PO_4F/C$ in the potential window of 3.0–4.5 V (*vs.* $Li/Li^+$). (b) shows the successive cycling at different rates after the tests in (a). The filled circles and hollow triangles designate the specific discharge capacities and the coulombic efficiencies (discharge capacity divided by charge capacity), respectively. The load density of the electrode is 1.67 mg $cm^{-2}$, with the formulation of active material : acetylene black : PVDF = 80 : 12 : 8 (weight).

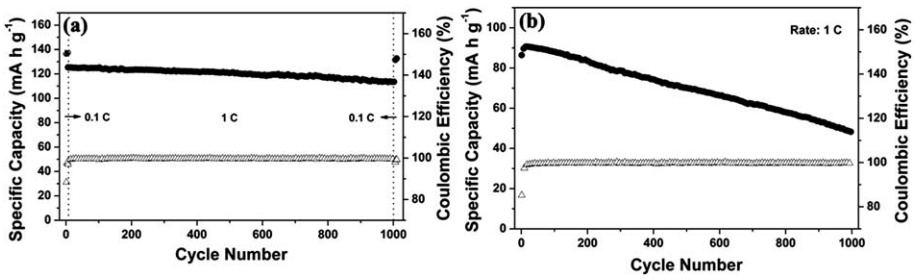


**Fig. 8** Room temperature cycling performance of $LiV_{0.96}Mn_{0.04}PO_4F/C$ (a) compared with $LiVPO_4F/C$ (b) between 3.0 and 4.5 V (*vs.* $Li/Li^+$). The filled circles and hollow triangles designate the specific discharge capacities and coulombic efficiencies, respectively. The load densities of the electrodes are 2.49 mg $cm^{-2}$ and 2.64 mg $cm^{-2}$in (a) and (b), respectively. Each electrode is composed of 80 wt% active material, 12 wt% acetylene black and 8 wt% PVDF.

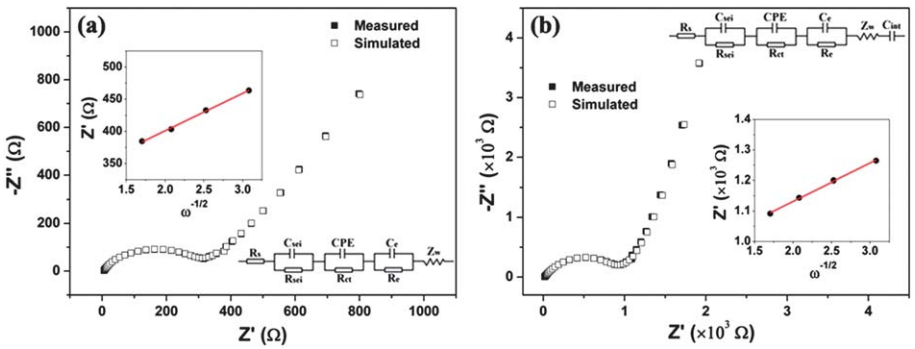


**Fig. 9** Room temperature EIS of $LiV_{0.96}Mn_{0.04}PO_4F/C$ (a) with comparison to that of $LiVPO_4F/C$ (b) at the discharged state after 10 cycles at 0.5 C. The data were collected after stabilizing for 2 h. The spectra are simulated by the equivalent electric circuits shown. The inset of each picture shows the $Z' \sim \omega^{-1/2}$ relationship in the low frequency region. The load densities of the electrode are 1.83 mg $cm^{-2}$ and 1.75 mg $cm^{-2}$in (a) and (b), respectively. Each electrode is composed of 80 wt% active material, 12 wt% acetylene black and 8 wt% PVDF.

shown by an inclined line in the low frequency region of the EIS. However, an insertion capacitance of $C_{int}$ corresponding to the accumulation and consumption of $Li^+$ in the active material is needed to fit the EIS of $LiVPO_4F/C$, which indicates irreversible lithium insertion/deinsertion during charge/discharge. From the simulated results (Table 2), the charge transfer resistance ($R_{ct}$) of $LiV_{0.96}Mn_{0.04}PO_4F/C$ (278.72 Ω $cm^2$) is found to be much lower than that of $LiVPO_4F/C$ (699.15 Ω $cm^2$).

The lithium diffusion coefficient ($D$) could be calculated by the following equation:

$$D = \frac{R^2T^2}{2A^2n^4F^4C^2\sigma^2} \quad (3)$$

where $R$ is the gas constant, $T$ is the temperature (K), $A$ is the surface area of the cathode, $n$ is the number of electrons per molecule involved in the redox reaction, $F$ is the Faraday constant, $C$ is the $Li^+$ concentration ($6.70 \times 10^{-3}$ mol $cm^{-3}$ for $LiV_{0.96}Mn_{0.04}PO_4F/C$ and $4.41 \times 10^{-3}$ mol $cm^{-3}$ for $LiVPO_4F/C$), and $\sigma$ is the Warburg factor that is associated with $Z'$:

$$Z' = R_D + R_L + \sigma\omega^{-1/2} \quad (4)$$

**Table 2** Impedance parameters of $LiV_{0.96}Mn_{0.04}PO_4F/C$ and $LiVPO_4F/C$

| | $R_{ct}$ ($\Omega$ cm$^2$) | $\chi^2$ | $\sigma$ ($\Omega$ cm s$^{-1/2}$) | $D$ (cm$^2$ s$^{-1}$) |
|---|---|---|---|---|
| $LiV_{0.96}Mn_{0.04}PO_4F/C$ | 278.72 | $3.25 \times 10^{-4}$ | 58.23 | $1.34 \times 10^{-13}$ |
| $LiVPO_4F/C$ | 699.15 | $2.31 \times 10^{-4}$ | 125.01 | $3.73 \times 10^{-14}$ |

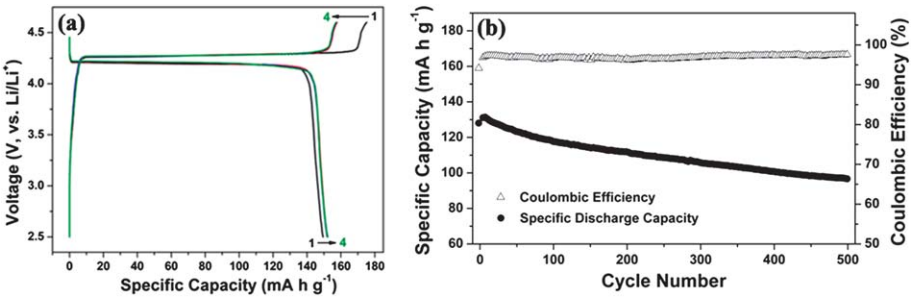


**Fig. 10** High temperature performance of $LiV_{0.96}Mn_{0.04}PO_4F/C$ at 65 °C. (a) Charge/discharge curves at 0.1 C, and (b) galvanostatic cycling between 3.0 and 4.5 V (*vs.* $Li/Li^+$) at a charge rate of 0.5 C and a discharge rate of 1 C. The load density of the electrode is 1.59 mg cm$^{-2}$ with the formulation of active material : acetylene black : PVDF = 80 : 12 : 8 (weight).

where $\omega$ is the frequency. The relationship of $Z'$ with the reciprocal square root of the frequency ($\omega^{-1/2}$) in the low frequency region is plotted in the inset of Fig. 9. The $Li^+$ diffusion coefficients of $LiV_{0.96}Mn_{0.04}PO_4F/C$ and $LiVPO_4F/C$ are thus calculated to be $1.34 \times 10^{-13}$ cm$^2$ s$^{-1}$ and $3.73 \times 10^{-14}$ cm$^2$ s$^{-1}$, respectively. The higher (one order of magnitude) $Li^+$ diffusion coefficient and the lower charge transfer resistance endow $LiV_{0.96}Mn_{0.04}PO_4F/C$ with higher capacity, more stable cyclability and fast charge/discharge capability.

Finally, the high temperature performance of $LiV_{0.96}Mn_{0.04}PO_4F/C$ was tested at 65 °C. The battery was first charge/discharged at 0.1 C between 2.5 and 4.6 V for 4 cycles. As shown in Fig. 10(a), the charge/discharge curves are ideal two-phase reaction profiles with extremely flat plateaus at 4.27 V and 4.21 V, respectively. The polarization is reduced and the specific capacity is increased compared with its performance at room temperature (Fig. 6), possibly due to the promoted reaction kinetics at high temperatures.[38] Note that the first cycle is still different from the others because of the formation of a SEI film. The battery was then charged at 0.5 C but discharged at 1 C between 3.0 and 4.5 V for 500 cycles to investigate its cycling performance. As shown in Fig. 10(b), the specific discharge capacity drops from 132 mA h g$^{-1}$ to 97 mA h g$^{-1}$ with a retention of 74%. Note that the temperature in Fig. 10 is 65 °C, which is higher than the widely used number (55 °C) for high temperature tests in the literature.[39] Therefore, $LiV_{0.96}Mn_{0.04}PO_4F/C$ is also anticipated to be a prospective high temperature cathode. It will hopefully improve the safety performance of LIBs, as well as those of the end applications such as electronic devices, HEVs, PHEVs, and ultimately EVs.

## 4 Conclusions

The specific capacity, rate performance and cycling stability of $LiVPO_4F$ are significantly improved by partial substitution of V with Mn in combination with *in situ* carbon coating *via* a facile modification of the CTR synthesis. The obtained $LiV_{0.96}Mn_{0.04}PO_4F/C$ also shows potential application at high temperatures. However, the detailed composition of the sample and the crystallographic structure at the atomic scale are still not clearly known. Further work needs to be done to fully understand the thermodynamic and kinetic process along with the lithium extraction/incorporation during charge/discharge.

## Acknowledgements

Xiaofei Sun would thank the Chinese Scholarship Council (CSC) for financial support, and the fruitful discussions with Dr J. Barker at Faradion Limited and Prof. G. Ceder at Massachusetts Institute of Technology. Kai Chen is supported by the NSFC (grant no. 50925104) and the 973 Program of China (grant no. 2010CB631003). Mrs Lijing Ma, Mrs Penghui Guo and Mrs Yanling Liu are appreciated for their technical help with XRD, XPS and SEM.

## References

1 M. S. Whittingham, *Chem. Rev.*, 2004, **104**, 4271.
2 H. Zhang, X. Yu and P. V. Braun, *Nat. Nanotechnol.*, 2011, **6**, 277.
3 K. S. Kang, Y. S. Meng, J. Breger, C. P. Grey and G. Ceder, *Science*, 2006, **311**, 977.
4 J. B. Goodenough and Y. Kim, *Chem. Mater.*, 2010, **22**, 587.
5 B. L. Ellis, K. T. Lee and L. F. Nazar, *Chem. Mater.*, 2010, **22**, 691.
6 P. Barpanda, M. Ati, B. C. Melot, G. Rousse, J. N. Chotard, M. L. Doublet, M. T. Sougrati, S. A. Corr, J. C. Jumas and J. M. Tarascon, *Nat. Mater.*, 2011, **10**, 772.

 

7 M. S. Islam, R. Dominko, C. Masquelier, C. Sirisopanaporn, A. R. Armstrong and P. G. Bruce, *J. Mater. Chem.*, 2011, **21**, 9811.
8 B. Kang and G. Ceder, *Nature*, 2009, **458**, 190.
9 G. Yang, J. R. Ying, J. Gao, C. Y. Jiang and C. R. Wan, *Rare Met. Mater. Eng.*, 2008, **37**, 936.
10 A. K. Padhi, K. S. Nanjundaswamy and J. B. Goodenough, *J. Electrochem. Soc.*, 1997, **144**, 1188.
11 J. Barker, M. Y. Saidi and J. L. Swoyer, *J. Electrochem. Soc.*, 2003, **150**, A1394.
12 F. Zhou, X. Zhao and J. R. Dahn, *Electrochem. Commun.*, 2009, **11**, 589.
13 B. L. Ellis, T. N. Ramesh, L. J. M. Davis, G. R. Goward and L. F. Nazar, *Chem. Mater.*, 2011, **23**, 5138.
14 J. M. Ateba Mba, C. Masquelier, E. Suard and L. Croguennec, *Chem. Mater.*, 2012, **24**, 1223.
15 J. Barker, R. K. B. Gover, P. Burns, A. Bryan, M. Y. Saidi and J. L. Swoyer, *J. Power Sources*, 2005, **146**, 516.
16 S. Y. Chung, J. T. Bloking and Y. M. Chiang, *Nat. Mater.*, 2002, **1**, 123.
17 J. R. Ying, M. Lei, C. Y. Jiang, C. R. Wan, X. M. He, J. J. Li, L. Wang and J. G. Ren, *J. Power Sources*, 2006, **158**, 543.
18 J. M. Tarascon and D. Guyomard, *Electrochim. Acta*, 1993, **38**, 1221.
19 R. J. Gummow, A. de Kock and M. M. Thackeray, *Solid State Ionics*, 1994, **69**, 59.
20 X. H. Ma, B. Kang and G. Ceder, *J. Electrochem. Soc.*, 2010, **157**, A925.
21 X. Li and Y. Xu, *Electrochem. Commun.*, 2007, **9**, 2023.
22 Q. Zhang, S. K. Zhong, L. T. Liu, J. Q. Liu, J. Q. Jiang, J. Wang and Y. H. Li, *J. Phys. Chem. Solids*, 2009, **70**, 1080.
23 J. Barker, R. K. B. Gover, P. Burns and A. Bryan, *Electrochem. Solid-State Lett.*, 2005, **8**, A285.
24 R. K. B. Gover, P. Burns, A. Bryan, M. Y. Saidi, J. L. Swoyer and J. Barker, *Solid State Ionics*, 2006, **177**, 2635.
25 J. Barker, M. Y. Saidi, R. K. B. Gover, P. Burns and A. Bryan, *J. Power Sources*, 2007, **174**, 927.
26 S. K. Zhong, Z. L. Yin, Z. X. Wang and Q. Y. Chen, *Rare Met.*, 2007, **26**, 445.
27 M. V. Reddy, G. V. Subba Rao and B. V. R. Chowdari, *J. Power Sources*, 2010, **195**, 5768.
28 H. Huang, T. Faulkner, J. Barker and M. Y. Saidi, *J. Power Sources*, 2009, **189**, 748–751.
29 S. K. Zhong, F. P. Li, J. Q. Liu, Y. H. Li and X. S. Deng, *J. Wuhan Univ. Technol., Mater. Sci. Ed.*, 2009, **24**, 552.
30 K. M. Shaju, G. V. Subba Rao and B. V. R. Chowdari, *Electrochim. Acta*, 2003, **48**, 1505.
31 H. Zhang, Z. Zhan and X. Liu, *J. Power Sources*, 2011, **196**, 8041.
32 G. Silversmit, D. Depla, H. Poelman, G. B. Marin and R. De Gryse, *J. Electron Spectrosc. Relat. Phenom.*, 2004, **135**, 167.
33 Y. L. Wang, X. K. Chen, M. C. Li, R. Wang, G. Wu, J. P. Yang, W. H. Han, S. Z. Cao and L. C. Zhao, *Surf. Coat. Technol.*, 2007, **201**, 5344.
34 N. Meethong, Y. H. Kao, S. A. Speakman and Y. M. Chiang, *Adv. Funct. Mater.*, 2009, **19**, 1060.
35 Z. Yan, S. Cai, X. Zhou, Y. Zhao and L. Miao, *J. Electrochem. Soc.*, 2012, **159**, A894.
36 M. V. Reddy, G. V. Subba Rao and B. V. R. Chowdari, *J. Mater. Chem.*, 2011, **21**, 10003.
37 E. Pollak, G. Salitra, V. Baranchugov and D. Aurbach, *J. Phys. Chem. C*, 2007, **111**, 11437.
38 Y. R. Zhu, Y. Xie, R. S. Zhu, J. Shu, L. J. Jiang, H. B. Qiao and T. F. Yi, *Ionics*, 2011, **17**, 437.
39 H. G. Jung, M. W. Jang, J. Hassoun, Y. K. Sun and B. Scrosati, *Nat. Commun.*, 2011, **2**, 516.